Experimental investigation of solitary breaking waves in the swash zone.

Lisa B. Smith[1], Atle Jensen[1], and Geir Pedersen[1]

[1] Department of Mathematics, University of Oslo, Norway

March 1, 2016

Abstract

This study presents an experimental investigation of plunging breakers on a sloping beach with an inclination of 5.1°. The incident waves are solitary waves with various amplitudes from non-breaking waves to plunging breakers, and the area investigated is the swash zone. PIV (Particle Image Velocimetry) is performed on images captured at four different field of views (FOV). The PIV measurements are compared with computed velocity fields from a Boundary Integral Model (BIM). There is excellent agreement between the experimental and the computed result for the non-breaking waves. The experimental results from the breaking waves indicate that the motion becomes more irregular as we move further up the beach. In addition, there seem to be more irregularities present for waves with larger amplitude. Shoreline position and maximum runup are measured, and are repeatable in both time and height, although cross-sectional variations of the shoreline shape are observed at maximum runup. Length and velocity of air bubbles entrapped by the plunger breakers are extracted from a image series captured with large a FOV. The images showed that a large air bubble seems to be stable for a time period during runup for the breaking waves.

1 Introduction

In shallow water with constant depth, the nonlinear effect and dispersion will be balanced for solitary waves (Peregrine, 1983). If the depth decreases as the wave travels towards the shore, the wave will steepen, and at some critical point breaking may occur. Breaking waves are one of the most important physical features in the swash zone (Elfrink and Baldock, 2002). Breaking waves have a large impact on sediment transport onshore, which can result in erosion on cliffs and affect construction located near the shore. Although breaking waves is a well-known phenomenon from our daily life, many physical aspects regarding wave breaking are still poorly understood.

Several experimental studies of breaking waves have been performed in the recent years. A broad range of different experimental methods have been utilized to measure quantities such as surface elevation, runup, shear stress, and velocities. Techniques such as Laser Doppler Velocimetry (Petti and Longo, 2001), PIV (Cowen et al., 2003) and shear sensors (Barnes et al., 2009) has been utilized. The swash zone is defined as the region where the beach is partly wetted during runup and rundown. Aeration and the small flow depth makes the swash zone a challenging region to study experimentally with the techniques mentioned above. A further development of the PIV method is Bubble image Velocimetry (BIV), which Rivillas-Ospina et al. (2012) use to investigate velocity fields in plunging breakers.

What did they find ?

Until now, PIV measurements with high resolution close to the beach have not been reported for breaking waves in the swash zone. This paper presents PIV measurements where the amplitude of the solitary breaking waves varies. The paper starts with a description of the

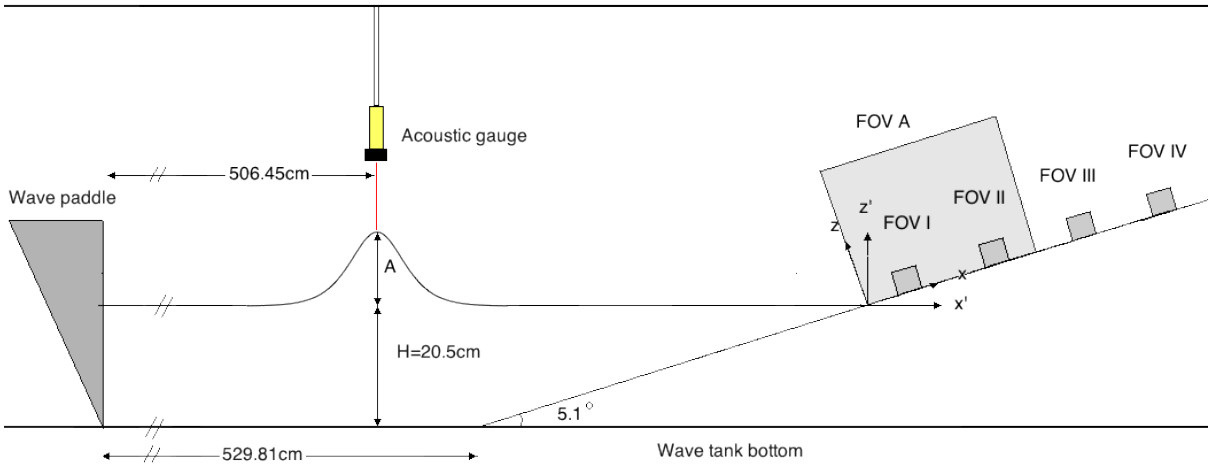

Figure 1: *Sketch of the experimental set-up.*

experimental set-up in chapter 2. Further on, results from different parts of the experiment will be presented, herein the surface elevation of the incident waves in chapter 3.1, surface development and maximum runup in chapter3.2, velocity profiles from the swash zone in chapter 3.3, and air bubble investigation in chapter 3.4. Finally, a discussion of the findings will be present in the last chapter 4.

2 Experimental set-up and formulation

2.1 The wave tank

Laboratory experiments of non-breaking to plunging breaking waves in the swash zone were conducted in a 25m long and 0.51m wide wave tank located at the Hydrodynamics Laboratory at the University of Oslo. Incident waves were generated in an equilibrium depth of 20.5cm by a piston type wave paddle using the method described in Jensen et al. (2003). A PETG (Polyethylene Terephthalate Glycol-modified) beach with an inclination of 5.1° was placed in the wave tank with its toe 529.81cm from the start position of the wave paddle. Two coordinate systems were introduced, one parallel to the still water level (x', z'), and one parallel to the beach (x, z) (See Figure 1). The origin of both is at the equilibrium shoreline.

Nominally, the amplitude to depth ratios, A/H, should equal (0.1,0.2,0.3,0.4,0.5). However, imperfection in the generation and frictional effects along the wave tank reduced the heights slightly. An acoustic wave gauge (ultra Banner U-Gage S18U, sample frequency of 200Hz) measured the wave height at the toe of the beach. After correcting for reflections (see ...) the amplitudes were found to be $A/H = (0.0989, 0.1191, 0.1981, 0.2958, 0.3939, 0.4874)$.

Are the amplitudes corrected ? The way this correction is made must be described.

2.2 Instrumentation, measurements

To obtain velocity fields in the swash zone, images were captured at four different field of views (FOV), located upward along the beach (Table 1). The different FOV's are denoted with roman numbers. The water in the tank was seeded with polymid particles with diameters of approximately 50 μm. A Quantronix Darwin Duo pulsed laser generated a light sheet parallel to the centreline of the wave tank, and a Photron SA5 high speed camera (1024 x 1024) synchronized with the laser, captured images of the illuminated particles. A Carl Zeiss Makro- Planer 2/50 zf lens was used. Images were collected at 3000 frames per seconds (fps). The image processing were performed in DigiFlow (Dalziel, 2006). PIV was performed using interrogation windows of 32 x 8 pixels with a 75% overlap. Oblong interrogation windows are beneficial in boundary

FOV:	I	II	III	IV
Location, x:	[8.49 - 13.04]	[36.35 - 40.26]	[77.55 - 81.53]	[117.76 - 121.80]
Location, z:	[-0.05 - 3.78]	[-0.16 - 3.54]	[-0.04 - 3.79]	[-0.85 - 3.09]

Table 1: *Location of the different FOVs in cm. The dimensions of the FOVs are approximately 4cm x 4cm.*

layer flow and have been employed previously in **?** and Pedersen et al. (2013). An averaging in time was applied where 10 images was used.

Are the averaging always 10?

To investigate air bubbles encapsulated by the plunging breakers, the camera was moved further away from the wave tank, resulting in much larger FOV than the FOVs installed to obtain velocity fields. This FOV will be referred to as FOV A and is located at $x = [0 - 60]$cm. 500 fps were used in this investigation, and a continuous dedolight 400D was used as illumination, replacing the laser. A white background sheet was attached to the side wall of the wave tank and the water was dyed dark blue to increase the contrast in the images.

The maximum runup was measured by capturing images of the shoreline at its maximum position. A high speed Photron APX camera was mounted on rails above the beach in the wave tank with same inclination as the beach. A high pulsed white light was used as illumination. The field of views were based on estimates of the runup height for each case. The camera captured 125 frames per second. The maximum shoreline profiles were tracked manually for each wave.

Each experiment was repeated at least three times. The scatter δ_i for some measured quantity, σ_i, is then calculated as,

$$\delta_i = \frac{\sigma_i - \overline{\sigma}}{\overline{\sigma}} \tag{1}$$

where $\overline{\sigma}$ is the mean over the repetitions.

2.3 The potential flow model

The evolution of the waves during shoaling, as well as the runup for the smallest amplitude, were computed by a BIM (Boundary Integral Model) for fully nonlinear, inviscid flow. This model breaks down when a plunger re-attaches with fluid or impacts the beach. Moreover, the model becomes singular when the contact angle at the shoreline exeeds 90° and the results also become unreliable for contact angles slightly smaller. More details are given in Pedersen et al. (2013).

Grid refinement?

3 Results

Visual inspection of the experiments revealed that the cases with normalized amplitude $A/H = 0.0989$ and $A/H = 0.1191$ did not break until the draw-down, while all the other cases developed into plunging breakers at or before the equilibrium shoreline. This is in compliance with numerical studies by Grilli et al. (1997). The plunger breakers encapsulated large amounts of air, which resulted in air bubbles in the swash tongue of the breaking waves (Figure 2).

cannot just say this, but mut give the breaking limit from Grilli et al

3.1 Surface elevation of the incident waves

The amplitude of the smallest amplitude wave is determined by a simple correction scheme. First the maximum of the series from the acoustic gauge is used as solitary wave amplitude in the BIM model. For the lowest wave this value is $\eta_m/H = ...$ When BIM data are extracted at the gauge position we then obtain a slightly too large surface elevation, due to the reflection from the beach, namely $\eta_b/H = ...$ We then adjust the amplitude according to $A = \eta_m - (\eta_b - \eta_m)$.

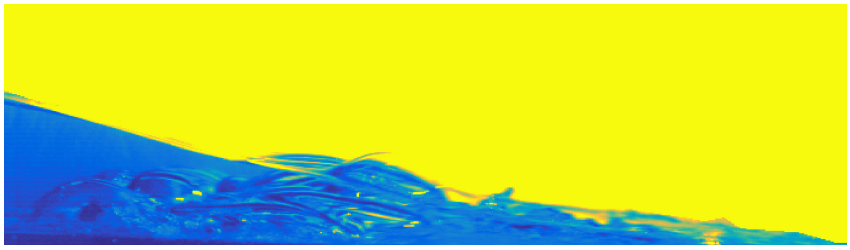

Figure 2: *Image of the swash tongue for* $A/H = 0.4874$.

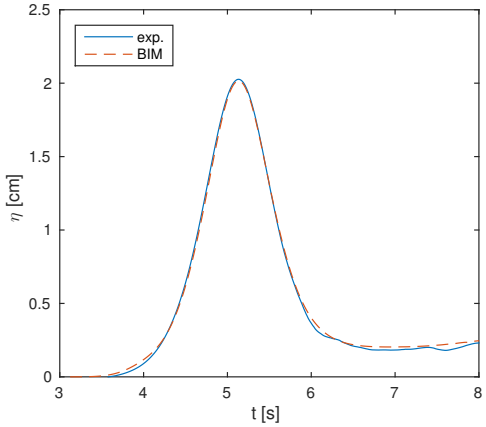

Figure 3: *Measured and computed surface elevation for* $A/H = 0.0898$.

The result is $A/H = 0.0989$ and the comparison with BIM results, obtained with this amplitude for the incident wave, is shown in Figure 3. Cubic polynomial regression is used to remove noise from the signal, and linear interpolation is used to fill in dropouts. The surface elevation measurements are in agreement with computed surface elevation from the BIM simulatitions.

Must explain why the dropouts are there and how reflection is corrected for.

3.2 Surface development and maximum runup

To investigate shoaling and runup of the waves both simulation and measurements have been conducted. BIM simulations of the near-shore evolution model is shown in figure 4). For reasons explained previously we only compute the runup for the smallest wave $A/H = 0.989$. The computed time and maximum runup height were were $t = 9.08$s and $r = 114.82$cm (measured along the beach), respectively. The BIM model had some difficulties with the waves with amplitude $A/H = 0.1191$. For the other cases shown the numerical model describes the evolution of the plunger, but nothing beyonds its impact onshore.

The measured maximum runup heights and deviations for each waves are available in Table 2. Both the time of maximum runup and the location seem to be over-predicted by the BIM simulation for the waves $A/H = 0.989$. The BIM model does not account for viscous effect in the simulations, and this may be the reason for the deviation between simulation and measurements. The Table shows that the maximum runup seemed to be repeatable for all waves including the breaking waves.

The shoreline at maximum runup are shown in Figure 5.It is fairly repeatable for the amplitue close to 0.1 times the depth (Figure 5a), but has a wedge-like shape. This is presumably due to a cross-wise deformation of the beach which has been measured using a straightedge and a feeling gauge. The maximum supression of the beach was 3.4mm and located at 2.0m from the origin in the middle of the cross section of the beach. The variation of 3.4 mm in the z direction should correspond to 3.4cm in the x direction since the beach slope is 1:10. It is clear from Figure 5 that the transverse variation is larger than this, which points to an

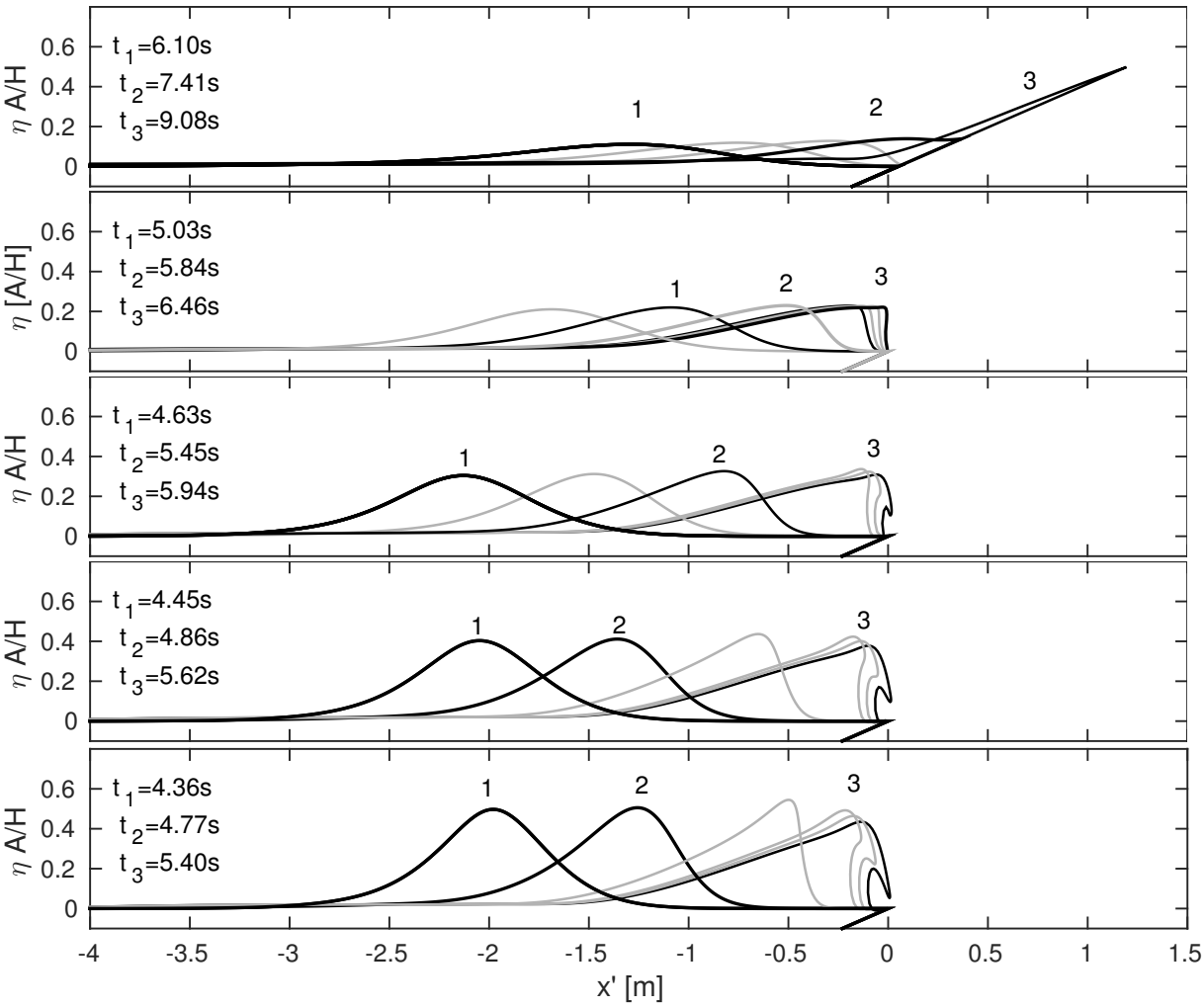

Figure 4: *BIM simulation of the waves the upper to lower figures correspond to* $A/H = (0.0989, 0.1981, 0.2958, 0.3939, 0.4874)$*, respectively. In the top panel the curve marked 3 corresponds to the time of maximum runup.*

A/H	S_o	$r[cm]$	R/A	$e_r[\%]$	t	$e_t[\%]$
0.0989	0.43	87.25	3.82	1.68	8.86 s	0.15
0.1191	0.39	105. 67	3.85	0.27	8.67 s	0.15
0.1981	0.30	147.37	3.22	0.93	8.53 s	0.31
0.2958	0.25	191.67	2.80	1.08	8.03 s	0.78
0.3938	0.22	227.42	2.50	0.11	7.82 s	0
0.4874	0.19	267.46	2.37	2.27	7.30 s	1.64

Table 2: *Maximum runup measurements where A/H is normalized amplitude, S_o is (Grilli et al., 1997) solitary wave breaking parameter, r is the runup in the direction along the beach, R is the vertical projection of the maximum runup, t is the time corresponding to max runup and e is the estimated error in the measurement*

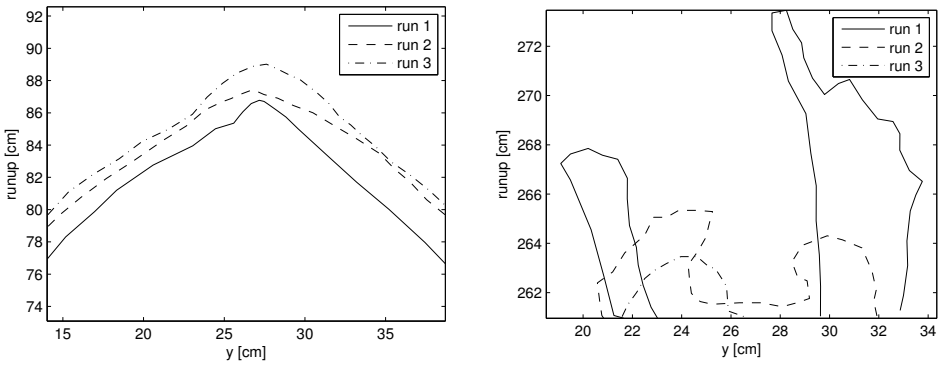

(a) $A/H = 0.0989$ (b) $A/H = 0.4874$

Figure 5: *Shoreline shapes at max runup.*

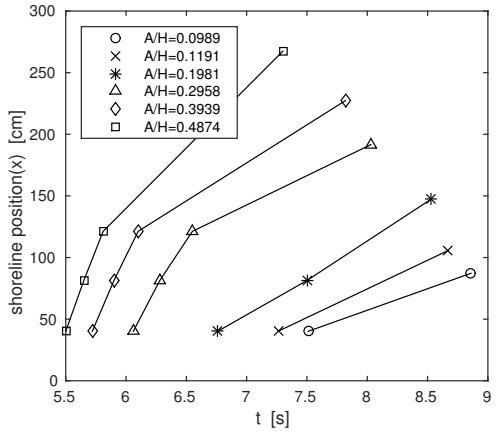

Figure 6: *Shoreline position as a function of time for all cases. The first measurements correspond to the swash tongue arrival time for FOV I, II, III. The last measuring point for all cases correspond to measurement of maximum runup*

accumulative effect. The runup varies much more for the three repititions of the breaking wave $A/H = 0.4874$, resulting in irregularly shaped shorelines (Figure 5b).

An estimate of the arrival time of the wave for FOV II, III and IV, were measured based on the intensity changes in images captured at each FOV. Each image in each time series was compared to the initial image taken before the wave paddle starts. The image where the sum of light intensity differs more than a given threshold (1000) from the initial image, correspond to the time when the wave enters that FOV. The measured shoreline positions as a function time are presented in Figure 6. The maximum error obtained for three different runs was 0.18%. This indicate that the shoreline motion was repeatable for each of the FOV.

3.3 Velocity profiles from the swash zone

Velocity profiles are extracted from the PIV data that are obtained from the four different FOV, approximately from 10cm to 120cm from the equilibrium shoreline. First, a comparison between computed BIM and measured PIV velocities for $A/H = 0.989$ will be given for FOV I and II, (See Figure 7). There is good agreement between measured and computed velocity profiles. The computed velocities are larger in the front of the wave for both the FOVs. This complies with corresponding results in Pedersen et al. (2013) where the delay of the experimental wave was linked to cappilary effects, while an accumulative reduction of velocity, and hence runup height, was related to the viscous bodary layers at the beach. Hence, the BIM computation

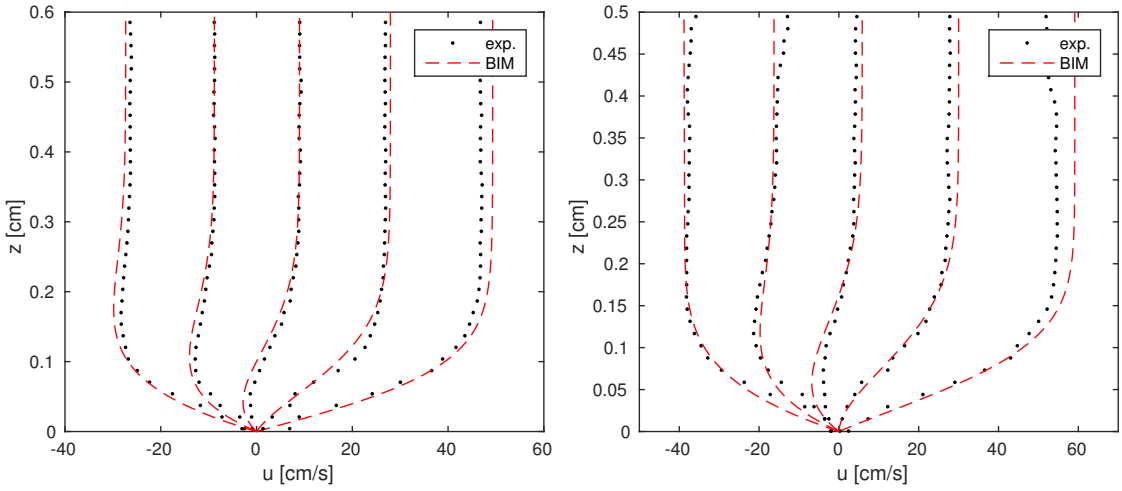

Figure 7:
Left: Velocity profiles from FOV I x=8.7cm t=[7.48, 7.82, 8.15, 8.48, 8.81]s
Right: Velocity profiles from FOV II x=40.1cm t=[7.76, 8.10, 8.76, 9.10]s

over-predicts the maximum runup as given in the previous section. Values ???

FOV II is located approximately 40cm from the origin, and velocity profiles obtained from this FOV are shown in Figure 8. For $A/H = 0.1981$ the particle density was too sparse close to the surface, which led to spurious vacillations in the velocity profiles near $z \approx 1$. An outer flow seems to be constant for both non-breaking and breaking waves. The event of a swash tongue moving with a constant velocity U upward a beach, can be compared to the problem of accelerating an infinite long plate from rest to a constant velocity U with a viscous fluid on top, Stokes first problem (White and Corfield, 2006). Dimensional analysis will then give us a relationship between the boundary layer thickness δ and the viscosity ν and the time t, $\delta \approx \sqrt{\nu t}$. This implies that the boundary layer will grow with time, and this seems to be the case for the small non-breaking waves with amplitude $A/H = 0.0989$ (Figure 7). However, for the strong plunging breakers the boundary layer decreases with time. This implies that the motion is more irregular than for the non-breaking waves.

FOV III is located about 80cm from origo along the beach. For $A/H = 0.0989$ and $A/H = 0.1191$, the swash tongues were too thin, and particles within the tongue were impossible to detect. Consequently, only $A/H = 0.1981 - 0.4874$ will be presented for this FOV. None of the cases had an outer flow with constant velocity at times close to outer flow reversal (Figure 9). This indicates that the motion was more irregular for this FOV than for FOV II.

FOV IV is located about 120cm from where the still water reaches the beach. At this FOV, only $A/H = 0.2958 - 0.4874$ will be presented due to the thin swash tongue for the other waves. Velocity profiles are given in Figure 10. The velocity was less repeatable at this location than for the other FOVs. The velocity profiles seemed to be more irregular, especially for $A/H = 0.4874$, where the average velocity profile obtained before flow reversal resembles the parbolic velocity profiles from fully developed turbulent channel flow, as described in White and Corfield (2006).

Inspection of movies of the front of the swash tongue from FOV IV (furthest up the beach) shows that a systematic swirling effect were present in the front of the swash tongue. Particle Tracking Velocimetry (PTV) have been utilized to investigate this phenomenon. Figure 11 shows how the velocities vary at one spot in fluid as a function of time. The velocities seem to oscillate, in addition to a linear decaying trend. The red line represents an interpolation of all the data, where 40 points are considered at each evaluation point. This indicates that there is a systematic velocity field in the front of the swash tongue.

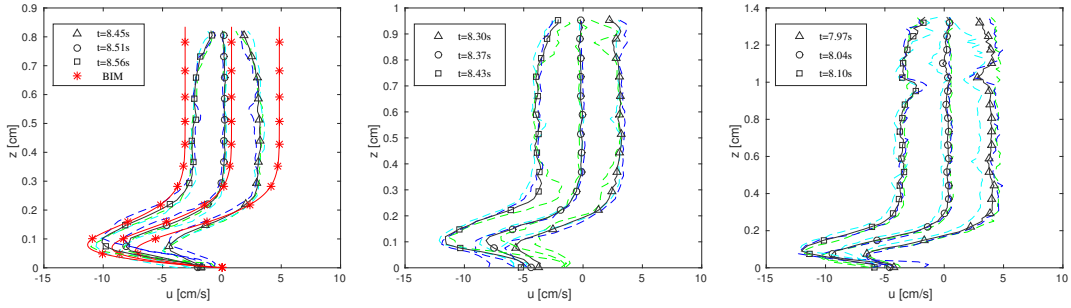

(a) $A/H = 0.0989$ (b) $A/H = 0.1191$ (c) $A/H = 0.1981$

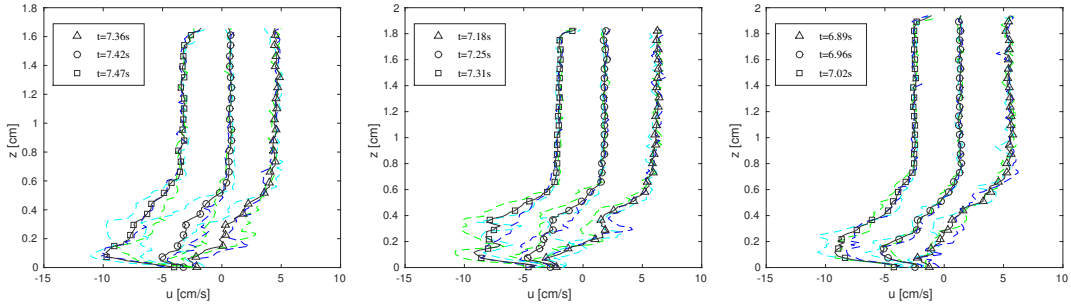

(d) $A/H = 0.2958$ (e) $A/H = 0.3939$ (f) $A/H = 0.4874$

Figure 8: *FOV II, mean velocity profiles before and after the outer flow reverses (△,□). Colors: blue, cyan, green and red correspond to run 1,2,3 and BIM respectively.* $x = 40.11cm$.

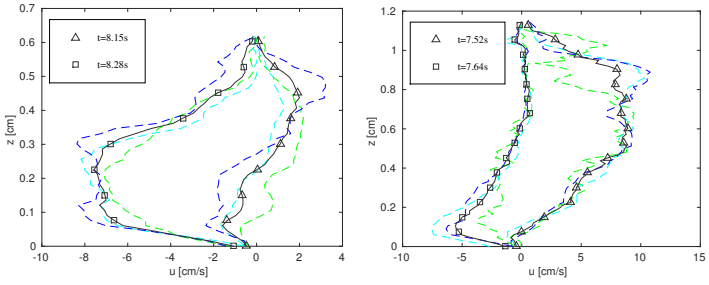

(a) $A/H = 0.1981$ (b) $A/H = 0.2958$

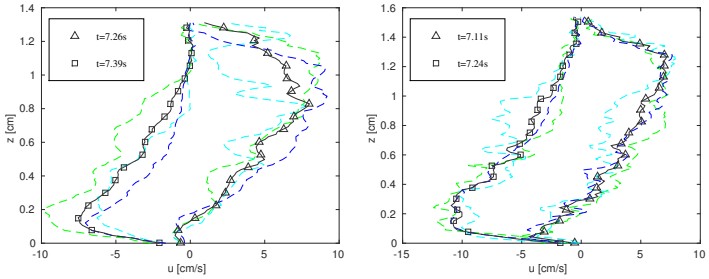

(c) $A/H = 0.3939$ (d) $A/H = 0.4874$

Figure 9: *FOV III, mean velocity profiles before and after the outer flow reverses (△,□). Colors: blue, cyan and green correspond to run 1,2 and 3.* $x = 81.40cm$

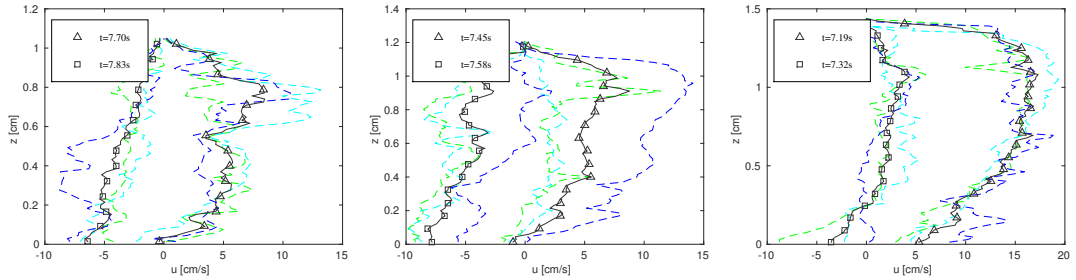

(a) $A/H = 0.2958$ (b) $A/H = 0.3939$ (c) $A/H = 0.4874$

Figure 10: *FOV IV, mean velocity profiles before and after the outer flow reverses (△,□). Colors: blue, cyan and green correspond to run 1,2 and 3.* $x = 121.25cm$

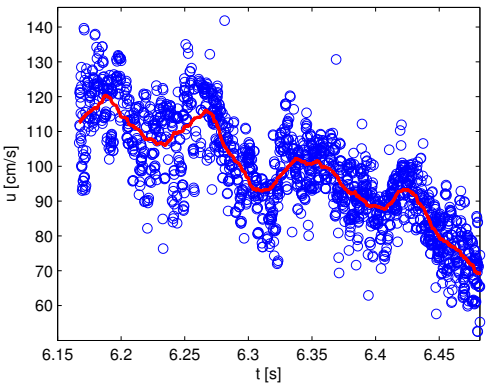

Figure 11: *FOV III Collection of velocities of particles within a distance of 0.05cm from the point(x,z)=(120,0.3)cm. The data is collected from* $A/H = 0.4874$*, run 2. Blue circles: Raw data points. Red line: 2 order interpolation with 40 evaluation points*

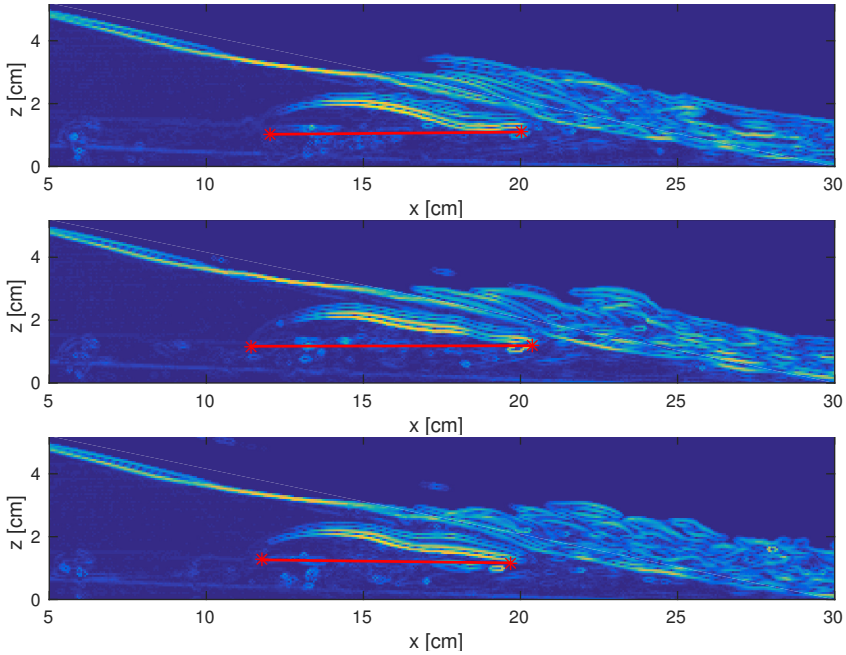

Figure 12: $A/H = 0.2958$, *run 1,2 and 3. t=6.06s*

Main bubble size	**Run 1 [cm]**	**Run 2 [cm]**	**Run 3 [cm]**
$A/H = 0.2958$:	8.00	8.94	7.90
$A/H = 0.4874$:	9.24		8.17

Table 3: *Size of the main bubble measured at t=6.06s for case 30, and t=5.54s for case 50*

3.4 Bubble investigation

For all the plunger breakers, the plunge encapsulated air, resulting in one large air bubble. As the waves propagated upward the beach, this large air bubble divided into smaller air bubbles, which again divided into even smaller air bubbles. Before reaching maximum runup, all the air bubbles had risen to the surface, for all waves. The images captured with the large FOV A provides some information about this air bubble formation, (see Figure 12 and 13). To enhance the shape of the bubbles the gradient magnitude image is represented. The shape of main bubble seems to be oval with a thin tongue in the front, for $A/H = 0.2958$. The shape of the main air bubble seems to vary more for $A/H = 0.4874$, especially for run2, where the large air bubble can't be found in the image. The length of the main bubble for three different runs is given in Table 3. It is clear that images from the three different runs for $A/H = 0.2958$ is more similar than for $A/H = 0.4874$. This supports the hypothesis that irregularity increases as normalized amplitude of the waves increases.

The air bubble velocity in the direction along the beach is given in Table 4. The largest velocities were obtained in the front of the bubbles, and may explain the shape of the thin tongue in the front of the air bubble observed for $A/H = 0.2958$. The bubble findings indicates that the motion becomes more irregular as the amplitude of the waves increases.

4 Discussion

The experimental result from the non-breaking waves generated in this study coincide with the numerical result from BIM model. Both, the surface elevation and velocities seems to agree with numerical result. However, deviations between the computed and the measured maximum

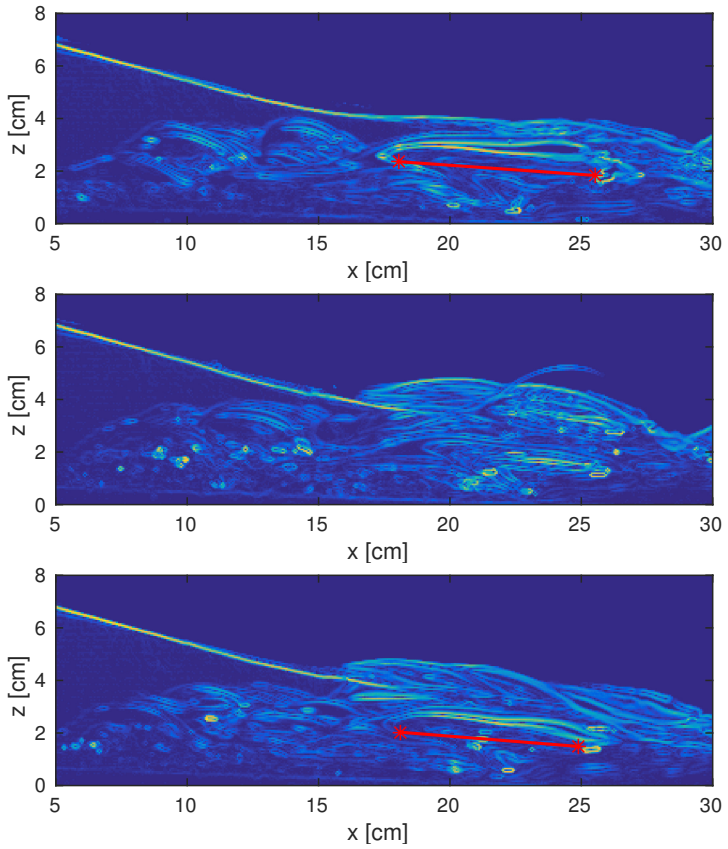

Figure 13: $A/H = 0.4874$, *run 1,2 and 3. t=5.54s*

$A/H = 0.2958$	Run 1	Run 2	Run 3
Front velocity [m/s]	2.05	2.20	2.48
Tail velocity [m/s]	2.10	2.05	2.23
$A/H = 0.4874$			
Front velocity [m/s]	3.26		2.01
Tail velocity [m/s]	1.58		2.23

Table 4: *Velocities along the beach for the main air bubble. t=6.06s for case 30, and t=5.54s for case 50*

runup was observed for the smallest waves. Also the BIM model over predict the velocity in front of the wave. Discrepancies between computation and measurement may be due to viscosity effect in the thin swash tongue, but may also be caused by bending effects of the beach. The beach bended due to its own weight and an additional bending was also observed due to wave load.

The measurement of the breaking waves showed that the fluid motion becomes more irregular and less repeatable as we move further up the beach. In addition, the motion seemed to be more irregular for the waves with the stronger plunger breakers than for those with smaller amplitude. The maximum runup was repeatable in both time and height, but large variation of the cross shore profiles was obtained for the breaking waves. The results from the bubble investigation showed that the air bubble seemed to be repeatable in shape for the waves with amplitude $A/H = 0.2958$ but not for waves with amplitude $A/H = 48.74$. Overall, irregular motion seems to increase with larger breaking waves and as the waves propagate upwards the beach.

Acknowledgment

This work was funded by the Research Council of Norway through the research project DOMT - Developments in Optical Measurement Technologies (project number 231491).

References

Barnes, M. P., O'Donoghue, T., Alsina, J. and Baldock, T. (2009), "Direct bed shear stress measurement in bore-driven swash", *Coastal Engineering* .

Cowen, E. A., A.M.ASCE, Sou, I. M., A.M.ASCE, Liu, P. L.-F., F.ASCE and Raubenheimer, B. (2003), "Particle image velocimetry measurements within a laboratory-generated swash zone", *J. Eng. Mech* .

Dalziel, S. B. (2006), 'Digiflow user guide', `http://www.damtp.cam.ac.uk/lab/digiflow/digiflow.pdf`. [Online; accessed 20-Aug-2014].

Elfrink, B. and Baldock, T. (2002), "Hydrodynamics and sediment transport in the swash zone: a review and perspectives", *Coastal Engineering* , Vol. 45, Elsevier, pp. 149–167.

Grass, A., Simons, R., Maciver, R., Mansour-Tehrani, M. and Kalopedis, A. (1995), "Shear cell for direct measurement of fluctuating bed shear stress vector in combined wave current flow".

Grilli, S., Svendsen, I. and Subramanya, R. (1997), "Breaking criterion and characteristics for solitary waves on slopes", *Journal of waterway, port, coastal, and ocean engineering* , Vol. 123, American Society of Civil Engineers, pp. 102–112.

Jensen, A., Pedersen, G. K. and Wood, D. J. (2003), "An experimental study of wave run-up at a steep beach", *Journal of Fluid Mechanics* , Vol. 486, Cambridge Univ Press, pp. 161–188.

Kikkerta, G., O'Donoghue, T., Pokrajacb, D. and Dodd, N. (2011), "Experimental study of bore-driven swash hydrodynamics on impermeable rough slopes", *Coastal Engineering* .

Pedersen, G., Lindstrøm, E., Bertelsen, A., Jensen, A., Laskovski, D. and Sælevik, G. (2013), "Runup and boundary layers on sloping beaches", *Physics of Fluids (1994-present)* , Vol. 25, AIP Publishing, p. 012102.

Peregrine, D. H. (1983), "Breaking waves on beaches", *Annual Review of Fluid Mechanics* , Vol. 15, Annual Reviews 4139 El Camino Way, PO Box 10139, Palo Alto, CA 94303-0139, USA, pp. 149–178.

Petti, M. and Longo, S. (2001), "Turbulence experiments in the swash zone", *Coastal Engineering* .

Rivillas-Ospina, G., Pedrozo-Acuña, A., Silva, R., Torres-Freyermuth, A. and Gutierrez, C. (2012), "Estimation of the velocity field induced by plunging breakers in the surf and swash zones", *Experiments in fluids* , Vol. 52, Springer, pp. 53–68.

Tanaka, M. (1986), "The stability of solitary waves", *Physics of Fluids (1958-1988)* , Vol. 29, AIP Publishing, pp. 650–655.

White, F. M. and Corfield, I. (2006), *Viscous fluid flow*, Vol. 3, McGraw-Hill New York.